Electrolyte Cation Effects on Interfacial Acidity and Electric Fields

Murielle F. Delley,[†,¶,*] Eva M. Nichols,[‡,¶] James M. Mayer[¶]

[†] Department of Chemistry, University of Basel, St. Johanns-Ring 19, 4056 Basel, Switzerland

[‡] Department of Chemistry, University of British Columbia, 2036 Main Mall, Vancouver, BC V6T 1Z1 Canada

[¶] Department of Chemistry, Yale University, New Haven, Connecticut 06520-8107, USA

murielle.delley@unibas.ch

Abstract. Electrolyte cation identity can have large effects on electrocatalysis by influencing the interfacial electric field, structure, or local pH. However, the specific role(s) of cations is not clear. Herein, we probed electrolyte cation effects on interfacial acidity and electric fields as a function of applied potential (ϕ_{app}) for mixed self-assembled monolayers (SAMs) of 4-mercaptobenzoic acid and 4-mercaptobenzonitrile on gold using Li^+, Na^+, K^+, ND_4^+, or tetrabutylammonium (TBA^+) phosphate electrolytes by surface-enhanced infrared absorption spectroscopy. The small cations showed only subtle differences in their effects on acidity and electric fields. In contrast, electrolytes containing the large TBA^+ gave much higher electric fields that were less sensitive to ϕ_{app}, and much more basic SAMs with a more ϕ_{app}-responsive p$K_{1/2}$. Varied cation identity and ϕ_{app} together can shift interfacial acid/base equilibria by >3 orders of magnitude. The impeded approach of TBA^+ to the surface results in less electric screening within the SAM and steeper potential decays into the electrolyte solution compared to other cations. Our data also suggest specific cation/surface COO^- interactions and cation identity effects on SAM heterogeneity. These insights on electrolyte cation effects on interfacial structure, proton transfer, and electric field are of fundamental interest for a range of electrochemical applications.

Introduction

Electrolyte cations can chemically interact with electrode surfaces, alter interfacial structures, and change the charge transfer ability at electrochemical interfaces.[1] Such cation effects are important for many electrocatalytic applications, including the electrochemical oxidations of hydrogen,[2] CO,[3] or methanol,[2] and the electrochemical reductions of oxygen,[2,4,5] CO,[6-8] or CO_2 (CO_2RR)[9-17] by metal electrodes. Cations affect the behavior of surface functionalities, from CO_2^- bound to a surface in the CO_2RR to carboxylate functionalities in surface ligands, as in self-assembled monolayers (SAMs) on metal electrodes. SAMs have long been viewed as valuable model systems to probe interfacial properties because of their relative homogeneity and the ease of including direct spectroscopic handles. While the importance of electrolyte cations is well known, the origin of these effects in electrocatalysis and interfacial properties is still debated.

One key element in the discussion of electrolyte cation effects is the adsorption mode of electrolyte cations at the electrode. In contrast to anions, cations are often thought to adsorb electrostatically and with intact hydration shells at the electrode surface. The location of the cations at the interface directly influences the key interfacial potential distribution.[18,19] In contrast to the normal behavior of anions, cyclic voltammetry does not typically show evidence of specific cation adsorption, i.e. direct metal-ion interaction with partial loss of the ion hydration shell. Specific or quasi-specific adsorption of cations has only been experimentally demonstrated in few cases, e.g. for Pt,[20,21] because obtaining direct evidence is challenging.[1,18,22] However, quasi-specific cation adsorption to the surface or a surface ligand has been a frequent proposal for the cation effects in electrocatalysis, for instance the binding to surface carboxylates as mentioned above.[2,10,13] Other proposals for electrolyte cation-dependent effects include changes in interfacial electric field and the interfacial potential distribution[9,15,23,24] and changes in the interfacial pH near the electrode.[11,25] A better understanding on how electrolyte cations adsorb, how the cation identity influences the interfacial electric field and the ability for proton transfer—a key elementary step in most electrocatalytic processes—is hence urgently needed.

The current study uses mixed carboxylic acid and nitrile-functionalized SAMs on gold electrodes to probe fundamental properties of the electrified interface. Prior studies of acidic SAMs have shown that they (de)protonate as a function of applied potential (ϕ_{app}), using cyclic voltammetry (CV),[26-30] or vibrational spectroscopic techniques.[30-37] Our own recent spectroelectrochemical study using surface-enhanced infrared adsorption spectroscopy (SEIRAS) of a 1:1 mixed SAM of 4-mercaptobenzoic acid (4-MBA) and 4-mercaptobenzonitrile (4-MBN) as a function of ϕ_{app} directly connected SAM acidity to the interfacial electric field.[38] Our results indicated that electrolyte cations have a key role in determining effective acidity at the electrified interface. In 500 mM sodium phosphate buffer, a 700 mV change in ϕ_{app} was needed to move the pK_a by one unit. This non-Nernstian relationship (non-59 mV/pK_a) is likely in large part due to cations penetrating the SAM and screening the potential within the SAM. Because of this, the potential difference from the acidic SAM edge to the bulk solution, the experienced potential ϕ_{exp}, is only a fraction of ϕ_{app}.

Theoretical models predict that it is this ϕ_{exp} that determines the effective acidity of the SAM via equation 1,[39,40]

$$pK_{1/2} = pK_a - \frac{F\phi_{exp}}{2.3RT} \qquad \text{(eq 1)}$$

where p$K_{1/2}$ and pK_a refer to the *effective* and *intrinsic* acidity of the SAM in presence and absence of an experienced potential, respectively, and F, R, and T refer to the Faraday constant, molar gas constant, and temperature, respectively. To test this model we previously employed the 4-MBN component of the SAM as a Stark reporter of the interfacial electric field, similarly to other studies.[38,41-48] The electric field is the derivative of potential with respect to distance. The shift of $\tilde{\upsilon}_{CN}$ with ϕ_{app} directly translates to the local electric field (E_F) via equation 2.[49-52]

$$\tilde{\upsilon}_{CN}\left(\overrightarrow{E_F}\right) = \tilde{\upsilon}_{CN}(0) - \Delta\vec{\mu} \cdot \overrightarrow{E_F} \qquad \text{(eq 2)}$$

In eq 2, $\tilde{\upsilon}_{CN}(0)$ = 2233.1 cm^{-1} is an estimate for the CN vibrational wavenumber of this mixed SAM in aqueous solution and in absence of an electric field[38] and $\Delta\mu$ is the difference in dipole moment between the ground and first excited vibrational states (the Stark tuning rate, estimated as $6.0 \cdot 10^{-9}$ cm^{-1}V^{-1}m as a first approximation, since the local field correction factor f is unknown. The actual $\Delta\mu$ is likely lower by a factor f of 1 to 2.).[41,49,53] Our analysis of the Stark data provided an estimate of ϕ_{exp} and implied that electrolyte cations contribute substantially to the interfacial charge density. Herein, we examine electrolyte cation effects on SAM-covered metal electrodes in detail.

The relevance of cation effects for SAM acidity has previously been implicated. Andreu and Fawcett suggested that cations should be treated as discrete charges to understand interfacial properties.[54] Experimentally, electrolyte cation effects on acidity have been studied e.g. by quartz microbalance or electrochemical methods, which showed similar responses for Na^+ and K^+ and larger effects for Ca^{2+}.[30,55] Rosendahl and Burgess reported the loss of voltammetric signal that has typically been connected to proton transfer events for a 4-MBA SAM in presence of electrolyte cations.[30] Those authors attributed this effect to disruption of interfacial hydrogen bonding and to cation exchange with protons. However, the absence or presence of CV waves for aromatic SAMs is not necessarily diagnostic of the chemistry occurring at the SAM interface.[38]

In sum, electrocatalysis on metal electrodes is clearly strongly influenced by cations and the more elementary studies on proton transfers by SAM-covered metal electrodes seem to imply cation effects as well. The development of improved electrochemical technologies could be accelerated by knowledge of cation adsorption modes and cation-effects on potential distribution and proton transfer reactivity at electrochemical interfaces. Here, we address these questions for a 1:1 4-MBA:4-MBN mixed SAM electrochemical interface by performing *in situ* SEIRA spectroscopy as a function of ϕ_{app} and solution pD with a series of different electrolyte cations.

Results

I. Overview.

A 1:1 4-MBA:4-MBN mixed SAM on gold was studied by SEIRAS as a function of ϕ_{app} and electrolyte solution pD in presence of 50 mM deuterated phosphate buffers with different cations:

Li^+, Na^+, K^+, ND_4^+, and tetrabutylammonium (TBA^+) (Figure 1). The 4-MBA and 4-MBN components of the SAM are intermixed and do not form separate domains as shown previously.[38] For each electrolyte cation we collected 3 or 4 replicate measurements, each with systematically varied electrolyte pD between 2 and 9 or 12, dependent on the cation, and varied ϕ_{app} from +300 to -400 mV vs Ag/AgCl. The ionic strength of the electrolyte solution was kept constant for the different cations and varied from ~10 to 150 mM across the examined pD range for each cation. We separately probed the effect of ionic strength in similar SEIRAS experiments on the mixed SAM by addition of NaCl aliquots. Cyclic voltammograms of the mixed SAMs using different electrolytes typically showed no (or only broad) voltammetric waves. Voltammetric waves have previously been observed for (de-)protonation events of alkyl SAMs,[26-29] but are not necessarily diagnostic of the occurrence such events as shown below.[38] It has been suggested that CV waves are more likely to be observed on closer to atomically flat gold surfaces versus the likely nanostructured Au from the sputtering technique used here.[56,57] See SI for further information on SAM preparation and experimental procedures.

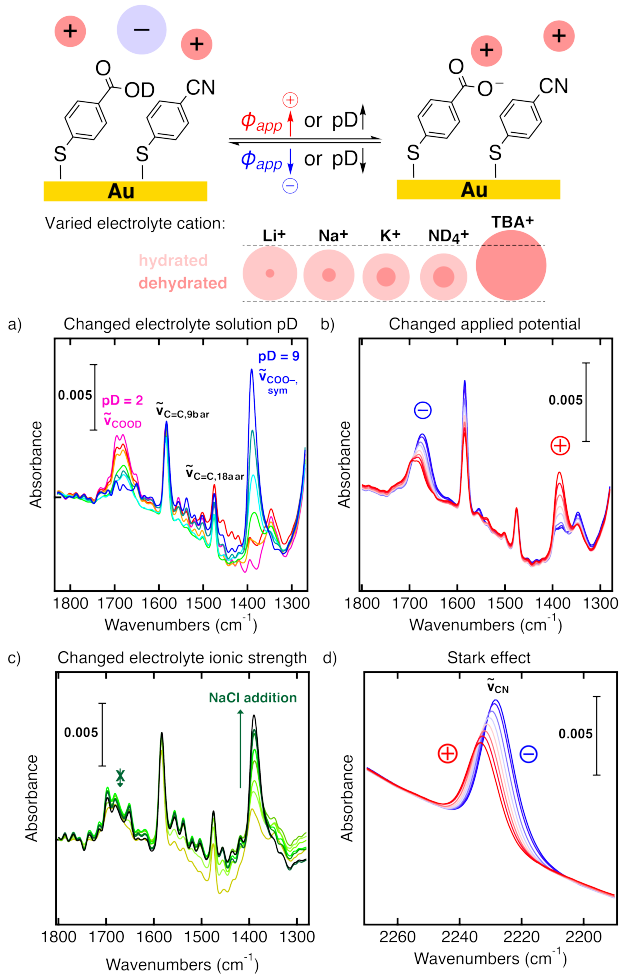

Figure 1. Top: Schematic of interfacial acid/base equilibrium that shifts with ϕ_{app} (vs Ag/AgCl) or solution pD. This equilibrium was probed as a function of electrolyte cation identity (Li^+, Na^+, K^+, ND_4^+, or TBA^+) and ionic strength. Relative hydrated and dehydrated cation sizes of the studied cations are shown below the scheme.[58] Panels: SEIRA

spectra of a 1:1 4-MBA:4-MBN mixed SAM in 50 mM phosphate buffer with ND_4^+ (a,b,d) or Na^+ (c) cations. Panels (a-c) show the region 1830-1270 cm^{-1} containing C=O stretching modes for COOD and COO^- headgroups, and aromatic ring stretching modes of the SAM. Panel (d) shows the region 2270-2190 cm^{-1} containing the CN stretching mode. (a) Varied pD from pD = 2 to 9 (rainbow colors), $\phi_{app} \cong -50$ mV; (b, d) varied ϕ_{app} = +250 to −400 mV (red to blue), pD = 6.7; (c) varied NaCl concentration changing ionic strength from ~10 to 1070 mM (light to dark green), $\phi_{app} \cong -50$ mV. Replicate data sets have been collected for all cations with solution pDs up to pD = 9 or 13.

The mixed SAM showed $\tilde{\upsilon}_{COOD}$ and $\tilde{\upsilon}_{COO^-}$ SEIRAS bands at ca. 1688 and 1384 cm^{-1}, respectively, characteristic of the 4-MBA COOD and COO^- surface groups in the SAM.[38] Following the $\tilde{\upsilon}_{COOD}$ and $\tilde{\upsilon}_{COO^-}$ band integrals relative to the fully protonated or deprotonated SAM at the low or high pD limits gave the interfacial COOD and COO^- fractional populations (see SI).[38] With all cation buffers studied, the COOD and COO^- fractional populations of the SAM varied as a function of solution pD and ϕ_{app} indicating acid/base equilibrium shifts (Figures 1a,b). This is similar to our previous results in 5 or 500 mM Na phosphate buffers.[38] In contrast, NaCl addition did not move intensity from one peak to the other, it only increased the $\tilde{\upsilon}_{COO^-}$ band integrals without affecting $\tilde{\upsilon}_{COOD}$ (Figure 1c). This suggested that the COOD/COO^- equilibrium was not shifted by increasing the Na^+ concentration (or, ionic strength). The observed increase of $\tilde{\upsilon}_{COO^-}$ band integrals may be caused by a change in IR absorption coefficient or – since SEIRAS bands are orientation-dependent[59] – a reorientation of the COO^- groups (e.g. by reordering of the SAM), perhaps through specific ion interaction with Na^+. An ordering effect by cations has previously been noted for Langmuir monolayers of fatty acids.[60]

The Stark reporter component in the mixed SAM, 4-MBN, can be identified by its $\tilde{\upsilon}_{CN}$ at ~2231 cm^{-1}.[38] For all cations, $\tilde{\upsilon}_{CN}$ of 4-MBN in the SAM varied mostly as a function of ϕ_{app} (rather than pD) indicating a Vibrational Stark Effect[49-52] of the interfacial electric field (Figure 1d).

II. Cation Effects on Surface Structures.

Acid/base Equilibria. Comparison of the relative $\tilde{\upsilon}_{COOD}$ and $\tilde{\upsilon}_{COO^-}$ band integrals and the derived fractional COOD and COO^- populations at a specific pD for varied electrolyte cations showed the cation effects on the 4-MBA acid/base equilibrium (Figure 2a and SI). Qualitatively, COOD:COO^- populations were roughly 50:50 at pD = 7 and ϕ_{app} = -50 mV vs Ag/AgCl for all smaller cations (Li^+, Na^+, K^+, and ND_4^+). With TBA^+, higher populations of COOD were obtained. The SAM carboxylic acids were hence less acidic in presence of TBA^+ than with other cations at the same ϕ_{app}. This showed that the relative acid/base populations and SAM acidity depended on electrolyte cation identity (see next section).

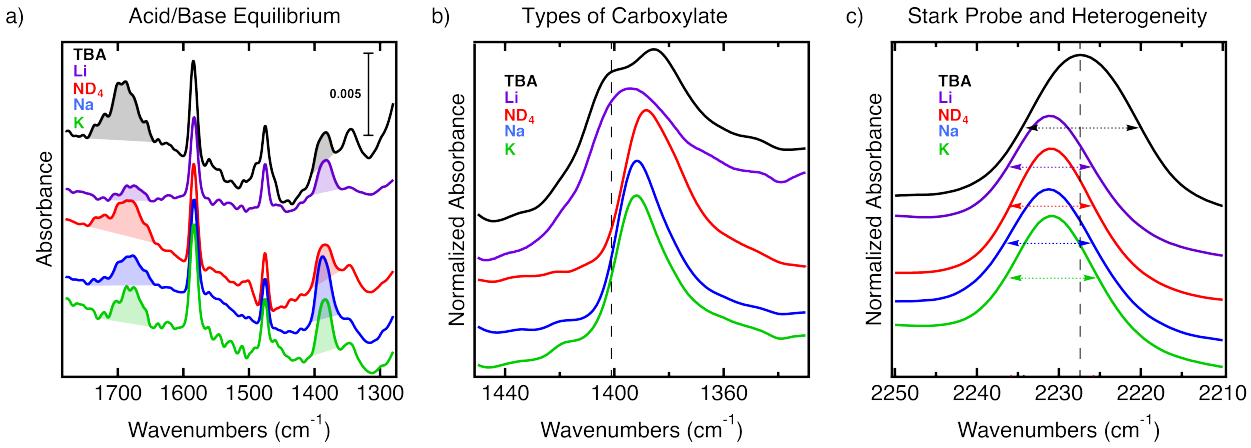

Figure 2. SEIRA spectra of a 1:1 4-MBA:4-MBN mixed SAM in 50 mM cation phosphate buffers at ~ −50 mV vs. Ag/AgCl, comparing the effect of electrolyte cation identity (TBA^+, black; Li^+, purple; ND_4^+, red; Na^+, blue; K^+, green). (a) Spectra showing acid/base equilibria, with a ~50:50 COOD:COO^- for most cations at pD = 7, higher COOD populations with TBA^+ (compare shaded $\tilde{\nu}_{COOD}$ and $\tilde{\nu}_{COO^-}$ band areas relative to each other for each cation). (b) Expansion of the carboxylate region of the spectra, showing only one $\tilde{\nu}_{COO^-}$ with Na^+, K^+, or ND_4^+, a broadened $\tilde{\nu}_{COO^-}$ with Li^+, and a second $\tilde{\nu}_{COO^-}$ (dashed line) with TBA^+ (high pD of 9 to 13, dependent on cation). (c) Expansion of the nitrile (Stark probe) region, with the TBA^+ spectrum showing a shifted $\tilde{\nu}_{CN}$ (dashed black line) with larger FWHM (horizontal double-arrows) vs other cations (pD = 7). Panels (b) and (c) show normalized absorbances. See SI for all replicate measurements for all cations.

Surface Carboxylates. The $\tilde{\nu}_{COO^-}$ band shape and width are indicative of the number and type of surface carboxylates present for different electrolyte cations (Figure 2b). At high pD (fully deprotonated SAM) the $\tilde{\nu}_{COO^-}$ band was broader with Li^+ buffers than with ND_4^+, Na^+, or K^+ buffers. This could be indicative of the presence of more than one type of carboxylate (though, the limited solubility of Li-phosphate in water may influence observations at high pD, see SI). A distribution of surface structures could for instance occur due to differing interaction strengths of carboxylates with Li^+, spanning weaker and stronger (specific) interactions.

Two distinct $\tilde{\nu}_{COO^-}$ were observed in TBA^+ buffers of high pD likely corresponding to at least two distinct types of carboxylates. The carboxylate associated with the higher energy $\tilde{\nu}_{COO^-}$ (at 1401 cm^{-1}) was absent in ND_4^+, Na^+, and K^+ buffers. We attribute this $\tilde{\nu}_{COO^-}$ present for TBA^+ (dashed line, Figure 2b) to a type of carboxylate that did not interact or that interacted only weakly with TBA^+ (i.e., at larger distances). This is consistent with literature on carboxylate-cation interactions in ionic liquids: a COO^-/TBA^+-system has two maxima in their anion-cation radial distribution functions at ~4 and 7 Å and shows two $\tilde{\nu}_{COO^-}$ bands.[61] Crystallographic data of COO^-/TBA^+ salts suggest similar N to O of TBA^+ to COO^- distances of 4–6 Å.[62-64] Metal carboxylate networks or ionic liquids with COO^-/Li^+ to COO^-/K^+, or COO^-/ND_4^+ have one carboxylate-cation distance ranging from 1.9 to 2.8 Å.[65-67] Since no weakly- or non-interacting carboxylate $\tilde{\nu}_{COO^-}$ were observed in presence of ND_4^+, Na^+, or K^+ buffers, these cations likely interacted by specific (strong) COO^-/cation-interactions with the SAM only.

Stark Reporter and Surface Heterogeneity. The $\tilde{\nu}_{CN}$ Stark data of 4-MBN reports on the local environment and the $\tilde{\nu}_{CN}$ band width can be indicative of the surface heterogeneity (Figure 2c). At any one ϕ_{app} and pD, the $\tilde{\nu}_{CN}$ frequency was remarkably similar for the smaller cations, while $\tilde{\nu}_{CN}$

was shifted to lower wavenumbers by 2-3 cm^{-1} for TBA^+ compared to the other cations. This reflects the higher electric field with TBA^+ (see the Stark response and discussion sections below). $\tilde{\upsilon}_{CN}$ was also significantly broader in presence of TBA^+ compared to the other cations, likely indicating a larger heterogeneity of the interface, consistent with the observation of multiple carboxylate stretches with this cation.

III. Effective Acidity as a Function of Applied Potential for Different Cations.

Under each set of conditions, the pD at which the relative COOD and COO^- surface populations are equal designates the effective acidity, p$K_{1/2}$, at this applied potential (ϕ_{app}) and buffer condition. (The procedure to normalize the spectra and extract p$K_{1/2}$ are described in our previous report.[38]) For all cations, the p$K_{1/2}$ depended linearly on ϕ_{app}, having higher p$K_{1/2}$ values at more negative ϕ_{app} (Figure 3). All p$K_{1/2}$ vs ϕ_{app} relationships were relatively shallow (<2.8 pD units/V, or >350 mV/pD). This shows that the potential experienced at the SAM surface by the carboxylic acids/carboxylates (ϕ_{exp}) is only a fraction of ϕ_{app} (see Discussion below and reference [38]). The absolute p$K_{1/2}$ values and the slopes of the p$K_{1/2}$ vs ϕ_{app} relationships varied with cation identity as described below. Notably, within the potential window examined and with varied cation the p$K_{1/2}$ of the same mixed SAM can vary from ~6.5 to 10, reflecting an acid/base equilibrium shift by more than three orders of magnitude.

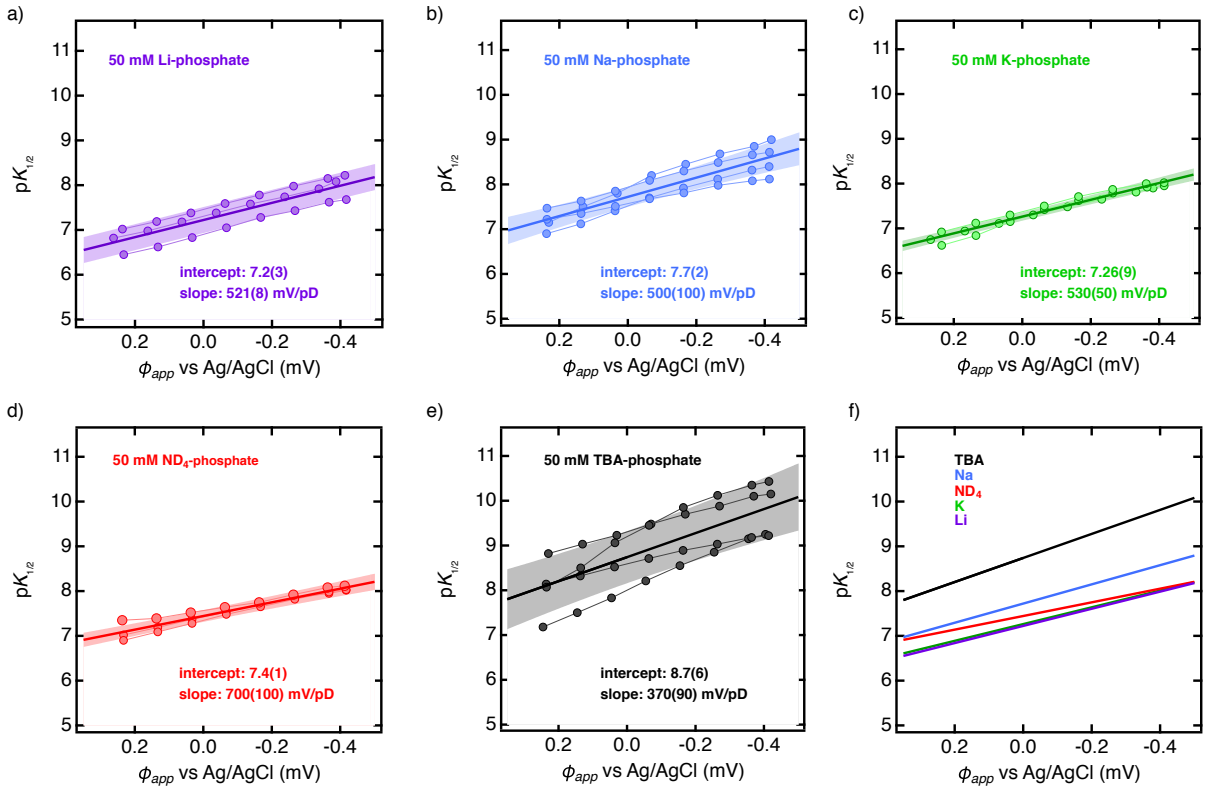

Figure 3. Plots of p$K_{1/2}$ (determined from relative surface populations of COOD and COO^-) vs ϕ_{app} for 1:1 mixed SAMs in 50 mM phosphate buffers with varied cation: a) Li^+, b) Na^+, c) K^+, d) ND_4^+, and e) TBA^+. Individual data sets (connected circles, three or four independent measurements) were fit linearly (not shown); Averages of these linear fits are shown as bold lines, in numerical values, and as a comparison for all cations in (f). Shaded areas designate the ±1σ uncertainty of these average relationships from propagation of the error in both slope and intercept.

Smaller cations. Li^+ and K^+ led to similar p$K_{1/2}$ vs ϕ_{app} relationships with a p$K_{1/2}$ of ~7.2 at 0 V vs Ag/AgCl and a slope of ~520 mV/pD (alternatively, 1.9 pD units/V). ND_4^+ led to similar acidity as Li^+ and K^+ within the examined potential window but with a shallower dependence on ϕ_{app} (700 mV/pD, or 1.4 pD units/V). Na^+ led to similar p$K_{1/2}$ vs ϕ_{app} slopes as Li^+ and K^+ (500 mV/pD) and a slightly more basic SAM (higher p$K_{1/2}$ by ca. 0.4) than ND_4^+, Li^+, and K^+. It is interesting that the SAM acidity was similar with Li^+ or K^+, but lower with Na^+ by 0.5(3) pK units. The SAM acidity hence does not correlate systematically with ion size for alkali cations in this system.

Large TBA^+. With TBA^+ phosphate buffers, the p$K_{1/2}$ of the SAM was much higher (8.7 at 0 V vs Ag/AgCl) and changed the most with ϕ_{app} (370 mV/pD, or 2.7 pD units/V), compared to the smaller cations. This is a significant cation effect even with the larger uncertainty for the p$K_{1/2}$ vs ϕ_{app} relationship in case of TBA^+. The larger uncertainty presumably reflects the larger structural heterogeneity with TBA^+ (see Figures 2b,c and corresponding text above). These data show that the SAM is much more basic and that the SAM acidity responds more sensitively to ϕ_{app} with TBA^+ compared to all other cations. This is consistent with weaker cation/COO^- interactions or weaker SAM penetration with the large TBA^+ (see Discussion).

IV. Stark Response for Different Cations.

After discussing the $\tilde{\upsilon}_{CN}$ width above, we here examine the Stark response – the variation of $\tilde{\upsilon}_{CN}$ as a function of ϕ_{app} – for different cations (Figure 4). The Stark reporter probes a 3D space at the interface around the CN group.[68] In this system, we previously identified this as the *interface region* likely containing the SAM COOD, COO^-, and CN headgroups, part of the SAM, and – particularly relevant here – nearby electrolyte components.[38]

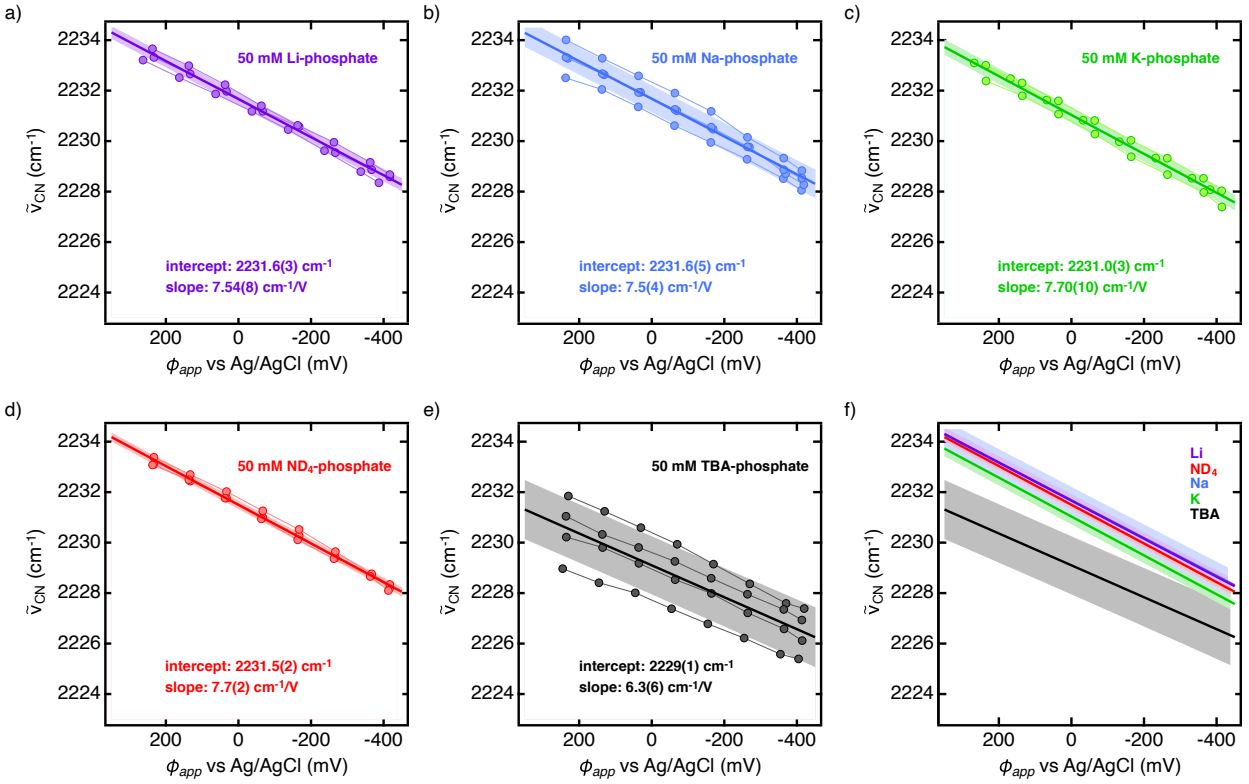

Figure 4. Plots of $\tilde{\upsilon}_{CN}$ vs ϕ_{app} for 1:1 mixed SAMs in 50 mM phosphate buffers at pD = 7 with varied cations: a) Li^+, b) Na^+, c) K^+, d) ND_4^+, and e) TBA^+. Individual data sets (connected circles, three or four independent measurements) were fit linearly (not shown); Averages of these linear fits are shown as bold lines, in numerical values, and as a comparison for all cations in (f). Shaded areas designate the ±1σ uncertainty of these average relationships from propagation of the error in both slope and intercept.

For all examined cations, $\tilde{\upsilon}_{CN}$ varied linearly with ϕ_{app}. The data for TBA^+ compared to other cations had a larger variation from one experiment to another, perhaps reflecting a greater sensitivity to small differences in SAM structure. The Stark response (both slope and intercept) was the same within error for ND_4^+, Li^+, and Na^+. The $\tilde{\upsilon}_{CN}$ vs ϕ_{app} slope varied with cation by $ND_4^+ \approx Li^+ \approx Na^+ \approx K^+$ (~7.6 cm^{-1}/V) > TBA^+ (6.3 cm^{-1}/V). A similar trend has previously been reported for CO-covered Cu electrodes showing shallower Stark slopes with larger electrolyte cations.[7]

Examination of the variation of the Stark intercept with different cations is particularly interesting, as our previous study showed that this is the most sensitive metric of local environment by Stark data.[38] This intercept is $\tilde{\upsilon}_{CN}$ at a fixed ϕ_{app}, here arbitrarily taken at 0 V vs Ag/AgCl. The Stark intercept trended with cation size: $ND_4^+ \approx Li^+ \approx Na^+$ (~2231.6 cm^{-1}) > K^+ (2231.0 cm^{-1}) > TBA^+ (2229 cm^{-1}). Note that this correlates with the non-solvated cation radii ($Li^+ < K^+ < TBA^+$) rather than the hydrated radii ($K^+ < Li^+ < TBA^+$) as shown in Figure 1,[58,69-72] suggestive of specific cation interactions with the SAM. Limited water access to the surface due to the hydrophobic TBA^+ could further contribute to the significantly shifted Stark intercept with TBA^+.[44,73] The Stark intercept shift observed here with TBA^+ vs other cations was even larger than Stark shifts previously observed with varied SAM surface composition.[38] This highlights the significance of electrolyte cations in determining the properties of the SAM and the interface.

Discussion

Our results show strong effects of cation identity on the SAM acidity and the Stark data, mostly for TBA^+ vs small cations. Switching the electrolyte cation to TBA^+ changed the SAM acidity by up to two p*K* units and the Stark response up to ~2.5 cm^{-1} at a specific ϕ_{app}. Small cations gave surprisingly similar SAM properties. Below we discuss (I) cation interactions with the SAM, (II) structural heterogeneity at the interface, (III) the volume probed by the Stark reporter, and (IV) cation effects on the interfacial potential distribution.

I. Cation Interaction with the SAM.

Since cation identity influenced interfacial properties, different cations likely interact with the SAM surface differently. Generally, this interaction can be specific with loss of the hydration shell, or non-specific with one or several intact hydration shells. The mode of interaction depends on whether ion-surface interactions or ion hydration energies dominate, and on other factors.[19] Cation interactions with the SAM are likely also pD- and potential-dependent,[1,74] and could potentially occur with any of the COOD, COO^-, and CN headgroups presented at the SAM surface.

The $\tilde{\upsilon}_{COO^-}$ band shapes for fully deprotonated SAMs indicated two distinct types of carboxylates only in presence of TBA^+. These likely stem from weak or strong interactions with TBA^+. Weak TBA^+/COO^- interactions are much more likely, as a consequence of the large TBA^+ size hindering its approach to the surface. This is supported by analysis of the p$K_{1/2}$ vs ϕ_{app} relationships. The much more basic SAM with TBA^+ compared to other cations indicates a decreased Coulombic stabilization of the COO^- with a cation and hence weaker interactions. In addition, the p$K_{1/2}$ response to ϕ_{app} is the largest with TBA^+. This indicates that a larger portion of ϕ_{app} is experienced by the acidic SAM headgroups and that ϕ_{app} is not screened as much across the SAM for TBA^+ (also see Discussion IV). These observations are consistent with the larger size of TBA^+ hindering cation-carboxylate association and/or SAM penetration. Displacement of interfacial water by the hydrophobic TBA^+ cations can also contribute to these observations.[7,75,76]

With Li^+, the observed broad $\tilde{\upsilon}_{COO^-}$ could indicate a distribution of interfacial structures spanning Li^+-SAM interactions with an intact first hydration shell or with loss of water(s) and

inner-sphere coordination of a SAM carboxylate. Li^+ has the largest hydration enthalpy among the cations,[72] and should be most prone to surface adsorption with an intact first hydration shell according to molecular dynamics (MD) simulations.[77]

The $\tilde{\upsilon}_{COO^-}$ band shapes at high pD further suggest that all cations can interact specifically (strongly) with the COO^- of the SAM and this is the exclusive mode of interaction for ND_4^+, Na^+, or K^+ cations. This is supported by the observed $\tilde{\upsilon}_{COO^-}$ SEIRAS intensity increase with added NaCl that presumably occurred through specific carboxylate-Na^+ interactions. Further support for specific cation interactions is provided by reported MD simulations for ion interactions with COO^--terminated SAMs.[77-79] Importantly, the Stark intercepts correlated with the non-hydrated cation radii rather than the hydrated radii. This suggests that the cations were at least partially dehydrated (e.g., fully dehydrated on one side or with loss of some of the 2nd-coordination sphere water molecules). These data further support specific cation interactions with the polarized SAM.

The small changes in p$K_{1/2}$ among the smaller cations could provide insight into subtle differences in specific interactions. The SAM p$K_{1/2}$ at any one ϕ_{app} does not correlate systematically with ion size among K^+, Na^+, and Li^+. This is quite unusual, but has sometimes been experimentally observed[80] and has been predicted by MD simulations for alkali ion interactions with COO^--terminated SAMs under certain conditions.[77] Non-ion-size-systematic effects cannot be simply explained by dominating ion-surface interaction or ion hydration energies,[78,81] but suggest other thermochemical contributions. For instance, non-ion-size-systematic effects might be due to action of matching water affinities, where ions prefer to pair with ionic groups with comparable hydration enthalpies.[80,82-84]

Among the small cations, the dependence of the p$K_{1/2}$ on ϕ_{app} was similar for alkali cations, but different for ND_4^+, which had the most stable (unresponsive) SAM acidity with ϕ_{app}. This might be due to interaction mechanisms that are only possible for ND_4^+, such as hydrogen-bonding.

Taken together, the data show that cations interact specifically with the SAM COO^- groups modulated by size, hydration energy, and binding mechanism. Spatial proximity of cations with CN groups is implied by the Stark data reporting on cation identity. We speculate that CN and COOD groups may be capable of non-covalent cation interactions (e.g. ion/dipole through-space interactions or H_2O-mediated hydrogen bonding), but this is currently not known. Specific interactions of cations with SAM COO^- or COOD headgroups seem reminiscent of the sometimes proposed stabilizing quasi-specific cation-metal electrode interactions via adsorbed COO^- or COOH intermediates during CO_2RR electrocatalysis,[10,13] or the non-covalent cation interactions with surface OH groups in Pt-based electrocatalysis.[2]

II. Structural Heterogeneity of the SAM.

The collected SEIRAS data provide information on the structural heterogeneity of the SAM as a function of electrolyte cation identity. The larger $\tilde{\upsilon}_{CN}$ width in presence of TBA^+ suggests a larger distribution of surface structures (i.e., a larger distribution of specific chemical environments for the CN groups). We attribute this to the larger cation size leading to less packed interfaces while small cations might reduce an inherent heterogeneity of the SAM through specific interactions. TBA^+ could also increase the heterogeneity of the interface due to its larger configurational

flexibility leading to a larger number of different stable interactions with the SAM. The $\tilde{\nu}_{COO^-}$ at high pD indicate two distinct classes of carboxylates in presence of TBA^+, and hence a heterogeneity in COO^- structures of bimodal character. Additional evidence for the structural heterogeneity with TBA^+ comes from the larger scatter in the p$K_{1/2}$ vs ϕ_{app} compared to other cations.

A larger structural heterogeneity for Li^+ compared to Na^+, K^+, and ND_4^+ is indicated by the broad $\tilde{\nu}_{COO^-}$ with this cation, as discussed above. In contrast to the case with TBA^+ this is neither reflected in the $\tilde{\nu}_{CN}$ band width, nor scatter in p$K_{1/2}$ vs ϕ_{app} relationships with Li^+. It is surprising that for Li^+ the heterogeneity seems to be limited to the carboxylates, while CN groups experience a relatively homogeneous environment—especially since our prior study has shown that the 4-MBA and 4-MBN components are well mixed in the SAM.[38]

III. Dimensions of the Interface Region.

As noted above, the Stark reporter probes a 3D *interface region* around the CN group containing SAM headgroups, likely part of the SAM, and electrolyte components.[38] Though Stark reporters have effectively and frequently been used,[38,41-47] the precise dimensions of this 3D space are not known. This knowledge would be valuable, however, as Stark data give information about the ensemble average of electrostatic contributions within this space that largely contribute in determining interfacial properties.[38,47,68] Here, we estimate the dimensions of this interface region for this system from Stark data with varied cation identity or ionic strength.

The fact that Stark response changed significantly only when going to electrolyte cations with large ionic radii (some change for K^+, large change for TBA^+, and correlation with dehydrated cation radii) may give some insight on these dimensions. Any structural changes at the interface potentially occurring with the electrolyte cations ND_4^+ vs Li^+ vs Na^+ were not distinguishable by this method. Hence, the ensemble of individual E_F vectorial contributions probed by the Stark reporter was the same within error for these cations. Large cations led to observable effects indicating a different spatial distribution of E_F contributions (all cations compared herein have a +1 charge). Our results may hence indicate that the 'reach' of the Stark probe extended far enough into the electrolyte solution to average the ND_4^+, Li^+, and Na^+ contributions, but not those of TBA^+. Based on reported COO^- oxygen-to-cation distances in other systems of 1.9-2.8 Å for COO^-/Li^+, K^+, and ND_4^+, or 4-7 Å for COO^-/TBA^+,[61-67] this seems to indicate a Stark probing depth into the electrolyte solution on the order of 3 Å.

Insight into the dimensions of the interface region into solution could also be obtained by analyzing the Stark response as a function of electrolyte ionic strength *I,* implemented by NaCl addition. The Stark slope was unaffected by varied *I*, and the Stark intercept was relatively constant for I = 300 to 1100 mM (shifts < –0.2 cm^{-1}, see SI). For low ionic strengths of I < ~300 mM the Stark intercept changed more significantly with *I* (shifted by ~–0.5 cm^{-1} between 0 and 300 mM). The interfacial potential screening by electrolytes of different ionic strength is typically described by a characteristic length-scale, the Debye length, at which the potential drops to its 1/*e* value.[18,19] Na phosphate buffers of I < 300 mM correspond to Debye lengths of >5.5 Å. This suggests that only at low electrolyte ionic strengths, when the cation-SAM surface characteristic length is larger than ~5.5 Å, did the Stark probe report a change.

Based on the combined results varying cation identity and ionic strength, we therefore estimate that the CN Stark reporter probes roughly 3-6 Å of interfacial electrolyte solution, and likely the SAM itself on similar length scales in a non-symmetric way around the CN.[68]

IV. Implications for the Interfacial Potential Distribution.

Based on the effective acidity and Stark data with varied ϕ_{app}, we here build on the model proposed previously[38] for a more detailed picture of the interfacial potential distribution as a function of electrolyte cation (Figures 5 and 6). This simplistic model was designed to only mirror the level of detail that is supported by our data. More complex treatments of electrochemical interfaces would likely include additional components, such as an explicit Stern layer,[85] or non-linear potential distributions within the SAM on an atomic level.[68]

Acidity and Experienced Potential. Classical theoretical models[39,40] predict that the SAM p$K_{1/2}$ depends in a Nernstian fashion on the experienced potential ϕ_{exp} (59 mV per pD, eq 1).[38] Experimentally, a one-unit change of p$K_{1/2}$ of the mixed SAM required 370-700 mV change in the applied potential ϕ_{app} for the various cations. This showed that the change in ϕ_{exp} ($\Delta\phi_{exp}$) is only 8-16% of the change in ϕ_{app} ($\Delta\phi_{app}$), similarly to what we and others proposed previously.[33,34,38] The significantly larger slope of p$K_{1/2}$ vs ϕ_{app} for TBA^+ compared to other cations indicates that changes in ϕ_{exp} with varied ϕ_{app} are larger in case of TBA^+ (Figure 5).

Insight into absolute values of ϕ_{exp} can be gained by examining specific ϕ_{app}'s and absolute values of observed p$K_{1/2}$ at a specific ϕ_{app}. At a $\phi_{app} = \phi_0$, ϕ_{exp} is zero and the interface region is uncharged.[38] ϕ_0 can be identified as the ϕ_{app} at which $\tilde{\upsilon}_{CN} = \tilde{\upsilon}_{CN}(0) = 2233.1$ cm^{-1} (see SI).[38,41] This occurs at a positive ϕ_{app} at or above +0.15 V vs Ag/AgCl for this mixed SAM with the cations studied. This means that within almost the full potential window examined here, the interface experiences a negative ϕ_{exp}. Therefore cations interact with the surface even at positive applied potentials ϕ_{app}. Notably, ϕ_0 is more positive by ca. +0.45 V for TBA^+ vs. other cations based on its higher ϕ_{app} at $\tilde{\upsilon}_{CN}(0)$. Therefore, a larger polarizing positive potential had to be applied in case of TBA^+ to get enough repulsive surface-cation Coulomb interaction to reach a net zero charge situation in the interface region. This is consistent with the expectation for larger cations having smaller charge densities and larger distance to the surface in the interface region and hence decreased Coulomb interactions. Secondly, at any one specific ϕ_{app}, the p$K_{1/2}$ with TBA^+ electrolytes was higher (more basic SAM) vs other cations. This indicates that ϕ_{exp} at any specific ϕ_{app} was more negative (larger in magnitude) for TBA^+ compared to the corresponding ϕ_{exp} with other cations (Figure 5).

In sum, the p$K_{1/2}$ vs ϕ_{app} relationships suggest that ϕ_{exp} is only a fraction of ϕ_{app} for all cations, and that ϕ_{exp} is more negative and changes more with ϕ_{app} for TBA^+ compared to other cations. This is illustrated in Figure 5. The less extensive potential screening across the SAM for TBA^+ is likely due to its size, which limits the interaction of TBA^+ with the SAM carboxylates and/or limits the penetration of TBA^+ into the SAM.

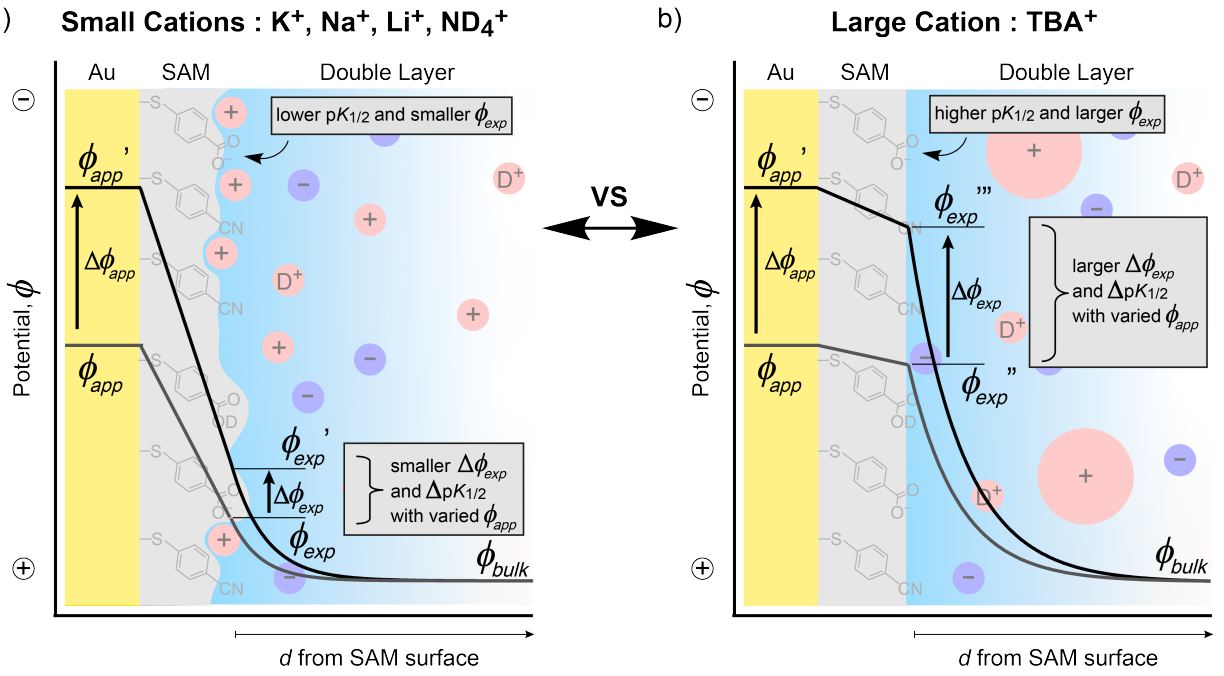

Figure 5. Cartoon of cation effects on the interfacial potential profile and SAM acidity: a) Smaller cations (K^+, Na^+, Li^+, and ND_4^+) can interact strongly with the SAM COO^- groups or penetrate the SAM (illustrated by a wavy SAM surface). b) In contrast, the large TBA^+ does not penetrate the SAM as well and on average does not come as close to the SAM surface (illustrated by a flat SAM surface). Compared to TBA^+, small cations hence led to a larger potential drop across the SAM and a shallower potential drop in the electrolyte solution (dark lines within grey and blue areas). Hence, the SAM had a lower $pK_{1/2}$ (more acidic) with a shallower dependence on ϕ_{app} with smaller cations.

Interfacial Electric Field. The observations made in the Stark results section with varied cation have likely two main contributors: an electrostatic effect due to cation-dependent changes in interfacial electric field and H-bonding effects due to cation-dependent changes in interfacial hydrophobicity.[44,49,73,86,87] To extract qualitative electrostatic trends, we here interpret the observed Stark responses as an electric field effect only and translate the Stark data into the ensemble-averaged electric field E_F in the interface region by equation 2.[41,43-46,49,50] The thereby determined E_F likely also contain cation-specific changes in the electrostatic contributions due to intermolecular interactions such as dipole-dipole interactions as we used a constant $\tilde{\upsilon}_{CN}(0)$ for the different cations in equation 2. E_F changed linearly with ϕ_{app} and varied between 0 and $-1.5 \cdot 10^9$ V m^{-1} (-1.5 V nm^{-1}) dependent on ϕ_{app} and cation (see SI). The measured E_F correspond to the average derivative of the potential with distance, $\frac{d\phi}{dd}$, around the Stark reporter in the interface region, as illustrated in Figure 6 (red dotted lines).

The similar Stark responses of the smaller cations, Li^+, Na^+, and ND_4^+, suggest similar ensemble averaged interfacial E_F with varied ϕ_{app}. At the same time, we obtained a shallower $pK_{1/2}$ vs. ϕ_{app} relationship with ND_4^+ vs other small cations. This implies a smaller $\Delta\phi_{exp}$ and a larger screening of the potential across the SAM for ND_4^+. The origin of this apparent contrast between similar E_F yet different potential screening is not clear. One should note, however, that the effective acidity of the SAM reflects differences in free energy between protonated and deprotonated states, while the Stark response gives an ensemble average of electrostatic contributions within the

interface region for the dominant state.[38] These are two different phenomena. The fact that one metric can distinguish between different cations while the other cannot highlights the utility of using two parallel probes of a system to obtain complementary information.

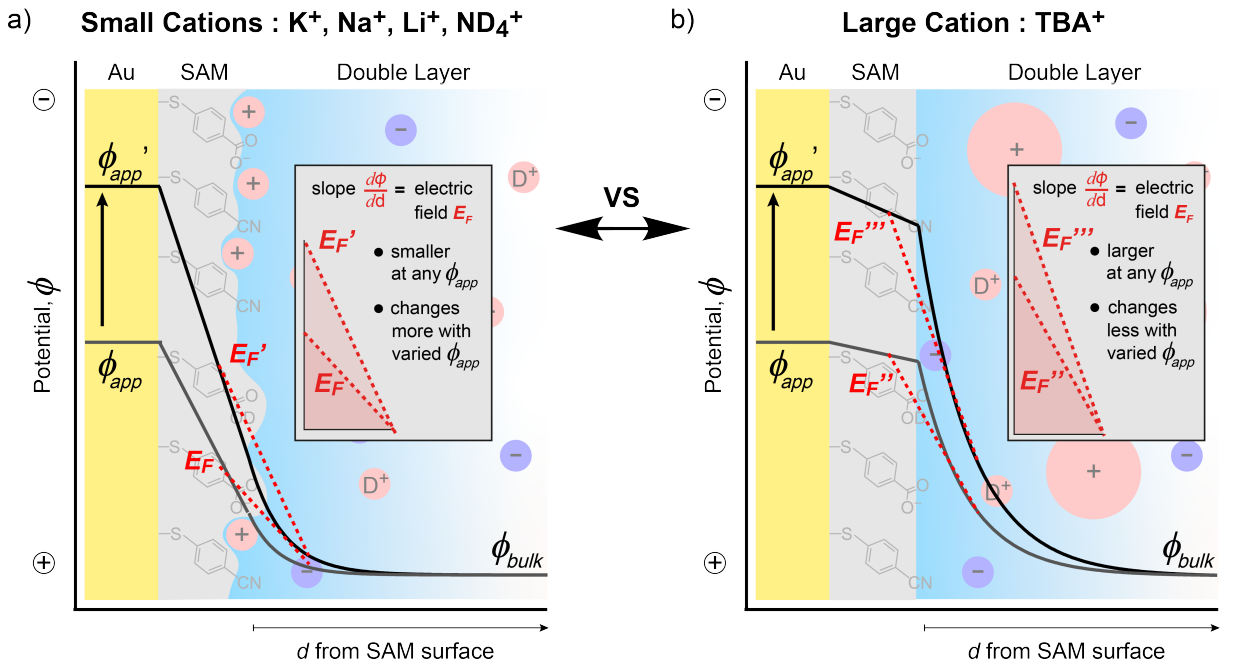

Figure 6. Cartoon of cation effects on the interfacial potential profile as in Figure 5, here highlighting interfacial electric fields. The electric field is the average derivative of potential with respect to distance (red dotted line) measured within the 3D interface region by the Stark probe. For small cations (a) this electric field is lower (less steep average slope), and the change of electric field with ϕ_{app} is larger (larger change in average slope) compared to (b) with the large TBA^+. The insets overlay these electric fields at different ϕ_{app} for small cations (a) or TBA^+ (b) for easier comparison. The differences result from the larger potential drop within the SAM for smaller cations.

The measured interfacial electric field was quite different with TBA^+ vs the other cations. The electric field in the interface region at a given ϕ_{app} is larger (more negative) for TBA^+ than for other cations (Figure 6). This means that ϕ_{app} is less screened *within* the SAM in presence of TBA^+ consistent with our $pK_{1/2}$ vs ϕ_{app} analysis above. A similar cation size effect has previously been reported for Me_3NR^+ surfactants at intermediate electrolyte concentrations of 0.5-10 mM by Dawlaty and coworkers.[47] Additionally to this electrostatic effect, the significantly shifted Stark response of TBA^+ to lower wavenumbers vs the other cations is likely in part due to the TBA^+'s larger hydrophobicity and decreased ability for H-bonding interactions.[44,49,73,86]

Furthermore, the smaller Stark slopes observed with TBA^+ vs small cations suggest that the electric field *changed less* with ϕ_{app} for the large TBA^+ (ΔE_F smaller) compared to other cations. This is illustrated in Figure 6, where the change in slope of the potential vs distance plots as a function of ϕ_{app} is smaller for TBA^+ than for other cations (compare among panel insets a and b, the differences in slope E_F at ϕ_{app} and ϕ_{app}'). Figures 6 and 5 also illustrate how $\tilde{\upsilon}_{CN}$ can change

less with ϕ_{app} (due to smaller ΔE_F), while the p$K_{1/2}$ changed more with ϕ_{app} (due to larger $\Delta\phi_{exp}$) for TBA^+ vs other cations.

Overall, the ϕ_{app}-dependent p$K_{1/2}$ and Stark response data combined suggest that both the potential drop across the SAM and outside towards bulk solution varied as a function of electrolyte cation identity. Interaction with the SAM surface and/or SAM penetration was less with the large TBA^+, which led to less potential screening across the SAM and this screening also varied less with ϕ_{app}. In the electrolyte solution outside the SAM, the potential therefore drops more steeply and the experienced potential changes more as a function of ϕ_{app} for TBA^+ vs small cations. These effects are likely general for bulky electrolyte cations.

Conclusions

Electrolyte cations extensively screened the applied potential and thereby strongly influenced the effective acidity (p$K_{1/2}$) and interfacial electric field (E_F) of acidic mixed SAMs on gold. Smaller cations (Li^+, Na^+, K^+, or ND_4^+) had very similar effects on p$K_{1/2}$ and E_F and their response to the applied potential ϕ_{app}. In contrast, dramatic changes were observed when switching to TBA^+ – much more basic SAMs, large acidity changes with ϕ_{app}, large negative E_F, and smaller E_F changes with ϕ_{app}. These effects show that the interfacial potential distribution is quite different with the large electrolyte cation: the potential drop is minimized across the SAM and maximized in solution due to the impeded approach of TBA^+ to and/or into the SAM surface.

Electrolytes with TBA^+ cations also had strong macroscopic effects on interfacial structure making it more heterogeneous than with smaller cations. For instance, two distinct types of SAM surface COO^- were observed with TBA^+. On a molecular level, there is evidence that Li^+, Na^+, K^+, or ND_4^+ associate specifically with the COO^- groups of this mixed SAM and lose part of their hydration shell. This is intriguing, because direct evidence for (quasi-)specific cation-metal electrode interaction has generally been difficult to obtain and is debated, e.g., for stabilization of surface-bound COO^- or COOH intermediates in CO_2RR electrocatalysis. Whether cations also interact with CN and/or COOD SAM surface groups or only with COO^- is not clear.

This study highlights how specific cation interactions influence interfacial structures, electric potential distribution, acidity, and charge transfer at electrified interfaces. By select choice of electrolyte cation identity and applied potential, the interfacial acid/base equilibria (and hence, the propensity for proton transfer) can be shifted by more than three orders of magnitude. These shifts are determined both by subtle effects of cation/carboxylate affinities and binding mechanisms, and by substantial effects through cation sterics. Similar cation phenomena could also contribute to the interfacial chemistry in electrocatalysis by metal electrodes or e.g. oxides with acidic functionalities. This work helps to understand cation effects at electrified interfaces that are relevant to a range of electrochemical applications, including electrocatalysis, (opto)electronic devices, or molecular electronics.

Associated Content

Supporting Information.

Detailed experimental procedures and infrared spectra are available in the SI.

Acknowledgments

This material is based upon work supported by the Air Force Office of Scientific Research under award number FA9550-18-1-0420 to a Multidisciplinary Research Program of the University Research Initiative (MURI) "Molecular-Scale Studies of Liquid-Solid Interfaces in Electrochemical Processes". Additional support was provided by the National Institutes of Health (NIH) under an Instrument Supplement grant 2R01GM050422. M.F.D. also gratefully acknowledges financial support from a Swiss National Science Foundation (SNSF) postdoctoral fellowship, a Swiss National Science Foundation (SNSF) PRIMA fellowship, and The Branco Weiss Fellowship – Society in Science, administered by the ETH Zürich. E.M.N. acknowledges the National Institutes of Health (NIH) for financial support under award number F32GM129902. The content is solely the responsibility of the authors and does not necessarily represent the official views of the National Institutes of Health.

References

1. Waegele, M. M.; Gunathunge, C. M.; Li, J.; Li, X., How cations affect the electric double layer and the rates and selectivity of electrocatalytic processes. *J. Chem. Phys.* **2019,** *151*, 160902.
2. Strmcnik, D.; Kodama, K.; van der Vliet, D.; Greeley, J.; Stamenkovic, V. R.; Marković, N. M., The role of non-covalent interactions in electrocatalytic fuel-cell reactions on platinum. *Nat. Chem.* **2009,** *1*, 466-472.
3. Stoffelsma, C.; Rodriguez, P.; Garcia, G.; Garcia-Araez, N.; Strmcnik, D.; Marković, N. M.; Koper, M. T. M., Promotion of the Oxidation of Carbon Monoxide at Stepped Platinum Single-Crystal Electrodes in Alkaline Media by Lithium and Beryllium Cations. *J. Am. Chem. Soc.* **2010,** *132*, 16127-16133.
4. Suntivich, J.; Perry, E. E.; Gasteiger, H. A.; Shao-Horn, Y., The Influence of the Cation on the Oxygen Reduction and Evolution Activities of Oxide Surfaces in Alkaline Electrolyte. *Electrocatalysis* **2013,** *4*, 49-55.
5. Strmcnik, D.; van der Vliet, D. F.; Chang, K. C.; Komanicky, V.; Kodama, K.; You, H.; Stamenkovic, V. R.; Marković, N. M., Effects of Li^+, K^+, and Ba^{2+} Cations on the ORR at Model and High Surface Area Pt and Au Surfaces in Alkaline Solutions. *J. Phys. Chem. Lett.* **2011,** *2*, 2733-2736.
6. Pérez-Gallent, E.; Marcandalli, G.; Figueiredo, M. C.; Calle-Vallejo, F.; Koper, M. T. M., Structure- and Potential-Dependent Cation Effects on CO Reduction at Copper Single-Crystal Electrodes. *J. Am. Chem. Soc.* **2017,** *139*, 16412-16419.
7. Li, J.; Li, X.; Gunathunge, C. M.; Waegele, M. M., Hydrogen bonding steers the product selectivity of electrocatalytic CO reduction. *Proc. Natl. Acad. Sci. U. S. A.* **2019,** *116*, 9220.
8. Gunathunge, C. M.; Ovalle, V. J.; Waegele, M. M., Probing promoting effects of alkali cations on the reduction of CO at the aqueous electrolyte/copper interface. *Phys. Chem. Chem. Phys.* **2017,** *19*, 30166-30172.
9. Murata, A.; Hori, Y., Product Selectivity Affected by Cationic Species in Electrochemical Reduction of CO_2 and CO at a Cu Electrode. *Bull. Chem. Soc. Jpn.* **1991,** *64*, 123-127.

10. Monteiro, M. C. O.; Dattila, F.; Hagedoorn, B.; García-Muelas, R.; López, N.; Koper, M. T. M., Absence of CO_2 electroreduction on copper, gold and silver electrodes without metal cations in solution. *Nat. Catal.* **2021,** *4*, 654-662.
11. Singh, M. R.; Kwon, Y.; Lum, Y.; Ager, J. W.; Bell, A. T., Hydrolysis of Electrolyte Cations Enhances the Electrochemical Reduction of CO_2 over Ag and Cu. *J. Am. Chem. Soc.* **2016,** *138*, 13006-13012.
12. Resasco, J.; Chen, L. D.; Clark, E.; Tsai, C.; Hahn, C.; Jaramillo, T. F.; Chan, K.; Bell, A. T., Promoter Effects of Alkali Metal Cations on the Electrochemical Reduction of Carbon Dioxide. *J. Am. Chem. Soc.* **2017,** *139*, 11277-11287.
13. Chen, L. D.; Urushihara, M.; Chan, K.; Nørskov, J. K., Electric Field Effects in Electrochemical CO_2 Reduction. *ACS Catal.* **2016,** *6*, 7133-7139.
14. Akhade, S. A.; McCrum, I. T.; Janik, M. J., The Impact of Specifically Adsorbed Ions on the Copper-Catalyzed Electroreduction of CO_2. *J. Electrochem. Soc.* **2016,** *163*, F477-F484.
15. Ringe, S.; Clark, E. L.; Resasco, J.; Walton, A.; Seger, B.; Bell, A. T.; Chan, K., Understanding cation effects in electrochemical CO_2 reduction. *Energy Environ. Sci.* **2019,** *12*, 3001-3014.
16. Thorson, M. R.; Siil, K. I.; Kenis, P. J. A., Effect of Cations on the Electrochemical Conversion of CO_2 to CO. *J. Electrochem. Soc.* **2012,** *160*, F69-F74.
17. Kyriacou, G. Z.; Anagnostopoulos, A. K., Influence CO_2 partial pressure and the supporting electrolyte cation on the product distribution in CO_2 electroreduction. *J. Appl. Electrochem.* **1993,** *23*, 483-486.
18. Schmickler, W., *Interfacial Electrochemistry*. 2nd ed.; Springer-Verlag: Berlin, 2010.
19. Bockris, J. O. M.; Reddy, A. K. N.; Gamboa-Aldeco, M., *Modern Electrochemistry, Fundamentals of Electrodics*. 2nd ed.; Kluwer Academic Publishers: New York, 2000; Vol. 2A.
20. Yamakata, A.; Soeta, E.; Ishiyama, T.; Osawa, M.; Morita, A., Real-time observation of the destruction of hydration shells under electrochemical force. *J. Am. Chem. Soc.* **2013,** *135*, 15033-9.
21. Chen, X.; McCrum, I. T.; Schwarz, K. A.; Janik, M. J.; Koper, M. T. M., Co-adsorption of Cations as the Cause of the Apparent pH Dependence of Hydrogen Adsorption on a Stepped Platinum Single-Crystal Electrode. *Angew. Chem., Int. Ed.* **2017,** *56*, 15025-15029.
22. Mills, J. N.; McCrum, I. T.; Janik, M. J., Alkali cation specific adsorption onto fcc(111) transition metal electrodes. *Phys. Chem. Chem. Phys.* **2014,** *16*, 13699-13707.
23. Frumkin, A. N., Influence of cation adsorption on the kinetics of electrode processes. *Trans. Faraday Soc.* **1959,** *55*, 156-167.
24. Hussain, G.; Pérez-Martínez, L.; Le, J.-B.; Papasizza, M.; Cabello, G.; Cheng, J.; Cuesta, A., How cations determine the interfacial potential profile: Relevance for the CO_2 reduction reaction. *Electrochim. Acta* **2019,** *327*, 135055.
25. Ayemoba, O.; Cuesta, A., Spectroscopic Evidence of Size-Dependent Buffering of Interfacial pH by Cation Hydrolysis during CO_2 Electroreduction. *ACS Appl. Mater. Interfaces* **2017,** *9*, 27377-27382.
26. White, H. S.; Peterson, J. D.; Cui, Q.; Stevenson, K. J., Voltammetric Measurement of Interfacial Acid/Base Reactions. *J. Phys. Chem. B* **1998,** *102*, 2930-2934.
27. Burgess, I.; Seivewright, B.; Lennox, R. B., Electric Field Driven Protonation/Deprotonation of Self-Assembled Monolayers of Acid-Terminated Thiols. *Langmuir* **2006,** *22*, 4420-4428.
28. Luque, A. M.; Mulder, W. H.; Calvente, J. J.; Cuesta, A.; Andreu, R., Proton Transfer Voltammetry at Electrodes Modified with Acid Thiol Monolayers. *Anal. Chem.* **2012,** *84*, 5778-5786.
29. Smiljanić, M.; Adam, C.; Doneux, T., Electric field induced proton transfer at α,ω-mercaptoalkanecarboxylic acids self-assembled monolayers of different chain length. *J. Electroanal. Chem.* **2018,** *815*, 238-245.
30. Rosendahl, S. M.; Burgess, I. J., Electrochemical and infrared spectroscopy studies of 4-mercaptobenzoic acid SAMs on gold surfaces. *Electrochim. Acta* **2008,** *53*, 6759-6767.

31. Michota, A.; Bukowska, J., Surface-enhanced Raman scattering (SERS) of 4-mercaptobenzoic acid on silver and gold substrates. *J. Raman Spectrosc.* **2003,** *34*, 21-25.
32. Gershevitz, O.; Osnis, A.; Sukenik, C. N., Interfacial chemistry on carboxylate-functionalized monolayer assemblies. *Isr. J. Chem.* **2005,** *45*, 321-336.
33. Ma, C.; Harris, J. M., Surface-Enhanced Raman Spectroscopy Investigation of the Potential-Dependent Acid−Base Chemistry of Silver-Immobilized 2-Mercaptobenzoic Acid. *Langmuir* **2011,** *27*, 3527-3533.
34. Ge, A.; Kastlunger, G.; Meng, J.; Lindgren, P.; Song, J.; Liu, Q.; Zaslavsky, A.; Lian, T.; Peterson, A. A., On the Coupling of Electron Transfer to Proton Transfer at Electrified Interfaces. *J. Am. Chem. Soc.* **2020,** *142*, 11829-11834.
35. Luque, A. M.; Cuesta, A.; Calvente, J. J.; Andreu, R., Potentiostatic infrared titration of 11-mercaptoundecanoic acid monolayers. *Electrochem. Commun.* **2014,** *45*, 13-16.
36. Futamata, M., Characterization of the first layer and second layer adsorbates on Au electrodes using ATR-IR spectroscopy. *J. Electroanal. Chem.* **2003,** *550-551*, 93-103.
37. Goutev, N.; Futamata, M., Attenuated Total Reflection Surface-Enhanced Infrared Absorption Spectroscopy of Carboxyl Terminated Self-Assembled Monolayers on Gold. *Appl. Spectrosc.* **2003,** *57*, 506-513.
38. Delley, M. F.; Nichols, E. M.; Mayer, J. M., Interfacial Acid–Base Equilibria and Electric Fields Concurrently Probed by In Situ Surface-Enhanced Infrared Spectroscopy. *J. Am. Chem. Soc.* **2021,** *143*, 10778-10792.
39. Smith, C. P.; White, H. S., Theory of the interfacial potential distribution and reversible voltammetric response of electrodes coated with electroactive molecular films. *Anal. Chem.* **1992,** *64*, 2398-2405.
40. Smith, C. P.; White, H. S., Voltammetry of molecular films containing acid/base groups. *Langmuir* **1993,** *9*, 1-3.
41. Schkolnik, G.; Salewski, J.; Millo, D.; Zebger, I.; Franzen, S.; Hildebrandt, P., Vibrational stark effect of the electric-field reporter 4-mercaptobenzonitrile as a tool for investigating electrostatics at electrode/SAM/solution interfaces. *Int. J. Mol. Sci.* **2012,** *13*, 7466-7482.
42. Ge, A.; Videla, P. E.; Lee, G. L.; Rudshteyn, B.; Song, J.; Kubiak, C. P.; Batista, V. S.; Lian, T., Interfacial Structure and Electric Field Probed by in Situ Electrochemical Vibrational Stark Effect Spectroscopy and Computational Modeling. *J. Phys. Chem. C* **2017,** *121*, 18674-18682.
43. Patrow, J. G.; Sorenson, S. A.; Dawlaty, J. M., Direct Spectroscopic Measurement of Interfacial Electric Fields near an Electrode under Polarizing or Current-Carrying Conditions. *J. Phys. Chem. C* **2017,** *121*, 11585-11592.
44. Sorenson, S. A.; Patrow, J. G.; Dawlaty, J. M., Solvation Reaction Field at the Interface Measured by Vibrational Sum Frequency Generation Spectroscopy. *J. Am. Chem. Soc.* **2017,** *139*, 2369-2378.
45. Shi, H.; Cai, Z.; Patrow, J.; Zhao, B.; Wang, Y.; Wang, Y.; Benderskii, A.; Dawlaty, J.; Cronin, S. B., Monitoring Local Electric Fields at Electrode Surfaces Using Surface Enhanced Raman Scattering-Based Stark-Shift Spectroscopy during Hydrogen Evolution Reactions. *ACS Appl. Mater. Interfaces* **2018,** *10*, 33678-33683.
46. Sarkar, S.; Patrow, J. G.; Voegtle, M. J.; Pennathur, A. K.; Dawlaty, J. M., Electrodes as Polarizing Functional Groups: Correlation between Hammett Parameters and Electrochemical Polarization. *J. Phys. Chem. C* **2019,** *123*, 4926-4937.
47. Sarkar, S.; Maitra, A.; Banerjee, S.; Thoi, V. S.; Dawlaty, J. M., Electric Fields at Metal–Surfactant Interfaces: A Combined Vibrational Spectroscopy and Capacitance Study. *J. Phys. Chem. B* **2020,** *124*, 1311-1321.
48. Oklejas, V.; Sjostrom, C.; Harris, J. M., SERS Detection of the Vibrational Stark Effect from Nitrile-Terminated SAMs to Probe Electric Fields in the Diffuse Double-Layer. *J. Am. Chem. Soc.* **2002,** *124*, 2408-2409.
49. Fried, S. D.; Boxer, S. G., Measuring Electric Fields and Noncovalent Interactions Using the Vibrational Stark Effect. *Acc. Chem. Res.* **2015,** *48*, 998-1006.

50. Slocum, J. D.; Webb, L. J., Measuring Electric Fields in Biological Matter Using the Vibrational Stark Effect of Nitrile Probes. *Annu. Rev. Phys. Chem.* **2018,** *69*, 253-271.
51. Staffa, J. K.; Lorenz, L.; Stolarski, M.; Murgida, D. H.; Zebger, I.; Utesch, T.; Kozuch, J.; Hildebrandt, P., Determination of the Local Electric Field at Au/SAM Interfaces Using the Vibrational Stark Effect. *J. Phys. Chem. C* **2017,** *121*, 22274-22285.
52. Sarkar, S.; Tseng, C.; Maitra, A.; Voegtle, M. J.; Dawlaty, J. M., Advances in Vibrational Stark Shift Spectroscopy for Measuring Interfacial Electric Fields. In *Emerging Trends in Chemical Applications of Lasers*, American Chemical Society: 2021; Vol. 1398, pp 199-224.
53. Schneider, S. H.; Boxer, S. G., Vibrational Stark Effects of Carbonyl Probes Applied to Reinterpret IR and Raman Data for Enzyme Inhibitors in Terms of Electric Fields at the Active Site. *J. Phys. Chem. B* **2016,** *120*, 9672-9684.
54. Andreu, R.; Fawcett, W. R., Discreteness-of-Charge Effects at Molecular Films Containing Acid/Base Groups. *J. Phys. Chem.* **1994,** *98*, 12753-12758.
55. Wang, J.; Frostman, L. M.; Ward, M. D., Self-assembled thiol monolayers with carboxylic acid functionality: measuring pH-dependent phase transitions with the quartz crystal microbalance. *J. Phys. Chem.* **1992,** *96*, 5224-5228.
56. Hatchett, D. W.; Stevenson, K. J.; Lacy, W. B.; Harris, J. M.; White, H. S., Electrochemical Oxidative Adsorption of Ethanethiolate on Ag(111). *J. Am. Chem. Soc.* **1997,** *119*, 6596-6606.
57. Stevenson, K. J.; Gao, X.; W. Hatchett, D.; White, H. S., Voltammetric measurement of anion adsorption on Ag(111). *J. Electroanal. Chem.* **1998,** *447*, 43-51.
58. Nightingale, E. R., Phenomenological Theory of Ion Solvation. Effective Radii of Hydrated Ions. *J. Phys. Chem.* **1959,** *63*, 1381-1387.
59. Osawa, M., Dynamic Processes in Electrochemical Reactions Studied by Surface-Enhanced Infrared Absorption Spectroscopy (SEIRAS). *Bull. Chem. Soc. Jpn.* **1997,** *70*, 2861-2880.
60. Johann, R.; Vollhardt, D.; Möhwald, H., Study of the pH dependence of head group bonding in arachidic acid monolayers by polarization modulation infrared reflection absorption spectroscopy. *Colloids Surf., A* **2001,** *182*, 311-320.
61. Khan, I. A.; Gnezdilov, O. I.; Wang, Y.-L.; Filippov, A.; Shah, F. U., Effect of Aromaticity in Anion on the Cation–Anion Interactions and Ionic Mobility in Fluorine-Free Ionic Liquids. *J. Phys. Chem. B* **2020,** *124*, 11962-11973.
62. Puranik, V. G.; Tavale, S. S.; Iyer, V. S.; Sehra, J. C.; Sivaram, S. The Cambridge Crystallographic Data Centre (CCDC): Deposition Number 1230757, 1994. (accessed 11.12.2021).
63. Puranik, V. G.; Tavale, S. S.; Iyer, V. S.; Sehra, J. C.; Sivaram, S., Tetrabutylammonium hydrogen bisbenzoate: crystal structure and study of short hydrogen bonds in hydrogen bisbenzoate anion system. *J. Chem. Soc., Perk. T. 2* **1993**, 1517-1520.
64. Light, M. E.; Brooks, S.; Gale, P. A. The Cambridge Crystallographic Data Centre (CCDC), Deposition number 1475647, 2016. (accessed 11.12.2021).
65. Pérez-Sánchez, G.; Santos, Y. S.; Ferreira, O.; Coutinho, J. A. P.; Gomes, J. R. B.; Pinho, S. P., The cation effect on the solubility of glycylglycine and N-acetylglycine in aqueous solution: Experimental and molecular dynamics studies. *J. Mol. Liq.* **2020,** *310*, 113044.
66. Asadi-Korayem, M.; Akbari-Taemeh, M.; Mohammadian-Sabet, F.; Shayesteh, A.; Daemi, H., How does counter-cation substitution influence inter- and intramolecular hydrogen bonding and electrospinnability of alginates. *Int. J. Biol. Macromol.* **2021,** *171*, 234-241.
67. Banerjee, D.; Parise, J. B., Recent Advances in s-Block Metal Carboxylate Networks. *Cryst. Growth Des.* **2011,** *11*, 4704-4720.
68. Goldsmith, Z. K.; Secor, M.; Hammes-Schiffer, S., Inhomogeneity of Interfacial Electric Fields at Vibrational Probes on Electrode Surfaces. *ACS Cent. Sci.* **2020,** *6*, 304-311.
69. Shannon, R., Revised effective ionic radii and systematic studies of interatomic distances in halides and chalcogenides. *Acta Crystallogr., Sect A* **1976,** *32*, 751-767.
70. Conway, B. E.; Ayranci, E., Effective Ionic Radii and Hydration Volumes for Evaluation of Solution Properties and Ionic Adsorption. *J. Solution Chem.* **1999,** *28*, 163-192.

71. Conway, B. E., The evaluation and use of properties of individual ions in slution. *J. Solution Chem.* **1978,** *7*, 721-770.
72. Mähler, J.; Persson, I., A Study of the Hydration of the Alkali Metal Ions in Aqueous Solution. *Inorg. Chem.* **2012,** *51*, 425-438.
73. Zhu, Q.; Wallentine, S. K.; Deng, G.-H.; Rebstock, J. A.; Baker, L. R., The Solvation-Induced Onsager Reaction Field Rather than the Double-Layer Field Controls CO_2 Reduction on Gold. *JACS Au* **2022,** *2*, 472-482.
74. Salaita, G. N.; Stern, D. A.; Lu, F.; Baltruschat, H.; Schardt, B. C.; Stickney, J. L.; Soriaga, M. P.; Frank, D. G.; Hubbard, A. T., Structure and composition of a platinum(111) surface as a function of pH and electrode potential in aqueous bromide solutions. *Langmuir* **1986,** *2*, 828-835.
75. Dubouis, N.; Serva, A.; Salager, E.; Deschamps, M.; Salanne, M.; Grimaud, A., The Fate of Water at the Electrochemical Interfaces: Electrochemical Behavior of Free Water Versus Coordinating Water. *J. Phys. Chem. Lett.* **2018,** *9*, 6683-6688.
76. Dubouis, N.; Serva, A.; Berthin, R.; Jeanmairet, G.; Porcheron, B.; Salager, E.; Salanne, M.; Grimaud, A., Tuning water reduction through controlled nanoconfinement within an organic liquid matrix. *Nat. Catal.* **2020,** *3*, 656-663.
77. Schwierz, N.; Horinek, D.; Netz, R. R., Specific Ion Binding to Carboxylic Surface Groups and the pH Dependence of the Hofmeister Series. *Langmuir* **2015,** *31*, 215-225.
78. Schwierz, N.; Horinek, D.; Sivan, U.; Netz, R. R., Reversed Hofmeister series—The rule rather than the exception. *Curr. Opin. Colloid Interface Sci.* **2016,** *23*, 10-18.
79. Schwierz, N.; Horinek, D.; Netz, R. R., Anionic and Cationic Hofmeister Effects on Hydrophobic and Hydrophilic Surfaces. *Langmuir* **2013,** *29*, 2602-2614.
80. Aziz, E. F.; Ottosson, N.; Eisebitt, S.; Eberhardt, W.; Jagoda-Cwiklik, B.; Vácha, R.; Jungwirth, P.; Winter, B., Cation-Specific Interactions with Carboxylate in Amino Acid and Acetate Aqueous Solutions: X-ray Absorption and ab initio Calculations. *J. Phys. Chem. B* **2008,** *112*, 12567-12570.
81. Parsons, D. F.; Boström, M.; Nostro, P. L.; Ninham, B. W., Hofmeister effects: interplay of hydration, nonelectrostatic potentials, and ion size. *Phys. Chem. Chem. Phys.* **2011,** *13*, 12352-12367.
82. Collins, K. D., The behavior of ions in water is controlled by their water affinity. *Q. Rev. Biophys.* **2019,** *52*, e11.
83. Collins, K. D.; Neilson, G. W.; Enderby, J. E., Ions in water: Characterizing the forces that control chemical processes and biological structure. *Biophys. Chem.* **2007,** *128*, 95-104.
84. Salis, A.; Bhattacharyya, M. S.; Monduzzi, M., Specific Ion Effects on Adsorption of Lysozyme on Functionalized SBA-15 Mesoporous Silica. *J. Phys. Chem. B* **2010,** *114*, 7996-8001.
85. Stern, O., Zur Theorie der elektrolytischen Doppelschicht. *Z. Elektrochem. angew. phys. Chem.* **1924,** *30*, 508-516.
86. Fafarman, A. T.; Sigala, P. A.; Herschlag, D.; Boxer, S. G., Decomposition of Vibrational Shifts of Nitriles into Electrostatic and Hydrogen-Bonding Effects. *J. Am. Chem. Soc.* **2010,** *132*, 12811-12813.
87. Deb, P.; Haldar, T.; Kashid, S. M.; Banerjee, S.; Chakrabarty, S.; Bagchi, S., Correlating Nitrile IR Frequencies to Local Electrostatics Quantifies Noncovalent Interactions of Peptides and Proteins. *J. Phys. Chem. B* **2016,** *120*, 4034-4046.

TOC Graphic

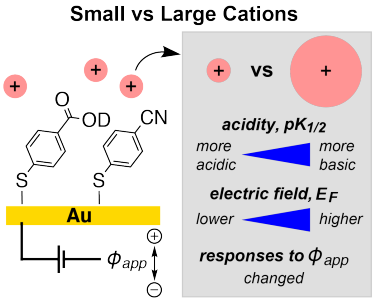
Small vs Large Cations
vs
acidity, pK1/2
more acidic
more basic
electric field, EF
lower
higher
responses to ϕapp changed
O
OD
CN
S
S
Au
ϕapp